

Connectivity in Random Grain Boundary Networks

M. Kumar, C.A. Schuh, W.E. King

This article was submitted to
The Metallurgical Society Annual Meeting 2003
San Diego, CA
March 2-6, 2003

October 22, 2002

U.S. Department of Energy

Lawrence
Livermore
National
Laboratory

DISCLAIMER

This document was prepared as an account of work sponsored by an agency of the United States Government. Neither the United States Government nor the University of California nor any of their employees, makes any warranty, express or implied, or assumes any legal liability or responsibility for the accuracy, completeness, or usefulness of any information, apparatus, product, or process disclosed, or represents that its use would not infringe privately owned rights. Reference herein to any specific commercial product, process, or service by trade name, trademark, manufacturer, or otherwise, does not necessarily constitute or imply its endorsement, recommendation, or favoring by the United States Government or the University of California. The views and opinions of authors expressed herein do not necessarily state or reflect those of the United States Government or the University of California, and shall not be used for advertising or product endorsement purposes.

This is a preprint of a paper intended for publication in a journal or proceedings. Since changes may be made before publication, this preprint is made available with the understanding that it will not be cited or reproduced without the permission of the author.

This report has been reproduced directly from the best available copy.

Available electronically at <http://www.doc.gov/bridge>

Available for a processing fee to U.S. Department of Energy
And its contractors in paper from
U.S. Department of Energy
Office of Scientific and Technical Information
P.O. Box 62
Oak Ridge, TN 37831-0062
Telephone: (865) 576-8401
Facsimile: (865) 576-5728
E-mail: reports@adonis.osti.gov

Available for sale to the public from
U.S. Department of Commerce
National Technical Information Service
5285 Port Royal Road
Springfield, VA 22161
Telephone: (800) 553-6847
Facsimile: (703) 605-6900
E-mail: orders@ntis.fedworld.gov
Online ordering: <http://www.ntis.gov/ordering.htm>

OR

Lawrence Livermore National Laboratory
Technical Information Department's Digital Library
<http://www.llnl.gov/tid/Library.html>

CONNECTIVITY IN RANDOM GRAIN BOUNDARY NETWORKS

Mukul Kumar¹, Christopher A. Schuh², and Wayne E. King¹

¹Lawrence Livermore National Laboratory, Livermore, CA 94550

²MIT, Department of Materials Science and Engineering, Cambridge, MA 02139

Abstract

Mechanical properties of FCC metals and alloys can be improved by exercising control over the population of grain boundary types in the microstructure. The existing studies also suggest that such properties tend to have percolative mechanisms that depend on the topology of the grain boundary network. With the emergence of SEM-based automated electron backscatter diffraction (EBSD), statistically significant datasets of interface crystallography can be analyzed in a routine manner, giving new insight into the topology and percolative properties of grain boundary networks. In this work, we review advanced analysis techniques for EBSD datasets to quantify microstructures in terms of grain boundary character and triple junction distributions, as well as detailed percolation-theory based cluster analysis.

Introduction

Grain boundaries and triple junctions exert significant influence on mechanical and physical materials properties. The effect of boundary character and crystallography and the grain boundary character distribution (GBCD) have been demonstrated for intergranular corrosion and cracking, creep behavior and cavitation characteristics, fracture toughness and plasticity, cold work embrittlement, and weldability.

An important aspect of assessing the optimization of the microstructure is to correlate microstructural parameters like the grain boundary character and triple junction distributions with the connectivity of grain boundary networks that are susceptible to failure. Wells et al. [1], on the basis of a bond percolation formulation, suggested that the probability of cracks propagating through the microstructure would be considerably reduced as the susceptible boundary fraction decreases below 0.65. This type of probabilistic analysis was further extended in the work of Palumbo et al. [2] to assess the crack resistance of a microstructure. This model was based on the fraction of crack-resistant grain boundaries, or the GBCD, but did not include consideration of the spatial arrangement of these special boundaries. The approach of Gertsman and Tangri [3] further combined both the percolation and Markovian description in a probabilistic methodology and they were able to predict percolation thresholds using both the grain boundary character and triple junction distributions. Interestingly, in all the above studies where a two-dimensional microstructure was assumed the threshold value of susceptible boundaries for crack propagation is about 0.65, which agrees closely with the value obtained from the bond-percolation calculation. The probabilistic nature of these approaches, however, does not fully incorporate the 2-point and higher order correlations that exist in a grain boundary network.

Advances in the engineering of grain boundaries in materials have been facilitated in recent years by the commercialization of automated electron backscatter diffraction (EBSD) techniques. This technique has largely superseded other experimental techniques for the determination of the GBCD, such as TEM and electron channeling in the SEM, due to the relatively straightforward specimen preparation and the large number of measurements attainable in a relatively short period of time. After acquisition and processing, EBSD data provide the x- and y-coordinates on a planar section, the three Euler angles of the underlying crystal, and a number of other parameters including the quality of the electron backscatter

diffraction pattern (EBSP) and the confidence in indexing. This allows the investigator to analyze many aspects of the microstructure, with spatial correlation of texture being a prominent example. This technique has also been instrumental for the field of grain boundary engineering, providing statistical information on grain boundary crystallography. In recent years, the use of EBSD has been extended to allow for more sophisticated analysis of the grain boundary network, including determination of triple junction distributions and mapping of the random grain boundary connectivity. This article attempts to summarize these new analysis techniques and highlight the main features of grain boundary networks.

Data Analysis: Strategies and Results

A brief discussion of data reduction methods and algorithms germane to 2-dimensional data sets is presented, with special emphasis on grain boundary networks. The EBSD data sets, acquired on a hexagonal grid, were analyzed using software developed using the IDL 5.5 (Research Systems, Inc. Boulder, CO) interactive data language program. The two-dimensional network of grain boundaries determined from EBSD data was analyzed by identifying boundary clusters, each cluster consisting of all the interconnected boundaries of like type, i.e., all random high-angle boundaries or all “special” CSL boundaries.

In a typical EBSD scan, some small fraction of the data points are of low “confidence index” (below a value of 0.1), indicating that the EBSP could not be unambiguously indexed [4]. Low confidence index points are more common near grain boundaries, where the diffracting volume may overlap two grains. Such points do not critically affect analyses of texture or grain boundary character distributions, but can markedly impact network connectivity, since a single low-confidence index point can divide a large cluster into two clusters of much smaller size. For quantitative analysis of cluster properties, it is therefore critical that the area fraction of these unindexed data points be as small as possible, and corrected to approximate the true crystallography in the specimen. In this work, a correction algorithm was employed to treat such data points, by assigning them the orientation of neighboring points of high confidence index.

The process of grain boundary engineering involves several cycles of straining and annealing [5,6], and increases the number fraction of special grain boundaries, f_n , as shown in

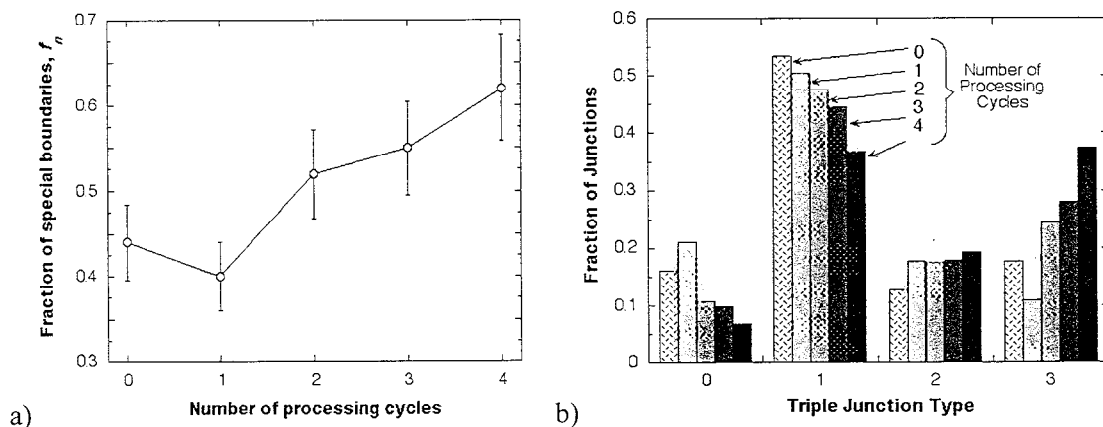


Fig. 1: a) Fraction of special grain boundaries by number, f_n , as a function of the number of cycles of rolling and annealing, and b) triple junction distributions corresponding to the number of special grain boundaries which coordinate the junction. The effect of sequential grain boundary engineering processing is also shown.

Fig. 1a for Inconel 600. This increase in special fraction is correlated with enhanced annealing twinning arising from boundary decomposition mechanisms [7]. The most quantitative measure of network connectivity previously described in the literature is the triple junction distribution [5,8], which gives information on the correlation of grain boundary types. Junctions are classified according to the number of special boundaries that coordinate them; type 0 junctions consist of 3 random boundaries, type 1, 2, and 3 junctions comprise, respectively, 1, 2, and 3 special boundaries. The triple junction distributions for Inconel 600 are shown in Fig. 1b as a function of grain boundary engineering processing cycles, and are similar to those reported previously for Cu and Inconel 600 [5]. The increase in type 2 and 3 junctions at the expense of types 0 and 1 reflects an increase in interconnectivity of special boundaries, and a concomitant decrease in the connectivity of random boundaries.

A more exhaustive analysis of boundary connectivity requires information about grain boundary clusters. In this work, such clusters were identified using a depth-first graph-search algorithm [9]. Essentially, a path of like boundary types (for example, a path of random boundaries) is followed through the microstructure, and branch points are identified and stored in a list. The current branch being followed can terminate in one of three ways: (i) at a triple junction coordinated by unlike boundaries, (ii) at the edge of the analyzed area, or (iii) by intersecting a boundary that has already been identified as part of the cluster (i.e., by closing a loop within the cluster). At any of these points, the search algorithm returns to a branch point in the list and proceeds down a new branch. The entire cluster is identified when a branch terminates and there are no more branch points stored in the list. An example of cluster identification is illustrated in Fig. 2, which shows the complete boundary network (random and special boundaries, Fig. 2a), only the random boundaries (Fig. 2b), and finally a single cluster isolated from the random boundary network (Fig. 2c). Before proceeding we note that the quantitative analysis to follow is performed in dimensionless units of length, where measured length is normalized by the mean linear intercept grain size, to facilitate comparison between microstructures.

Individual clusters are identified by their size and shape using standard measures from percolation theory [10]. The mass of a cluster, s , is defined as the total (dimensionless) length of boundary contained in the cluster. A mass close to unity likely represents a single, isolated boundary with no neighbors of the same type, while a large mass (i.e., several tens or hundreds) spans many grains, although its shape is unspecified by the mass alone. For a cluster composed

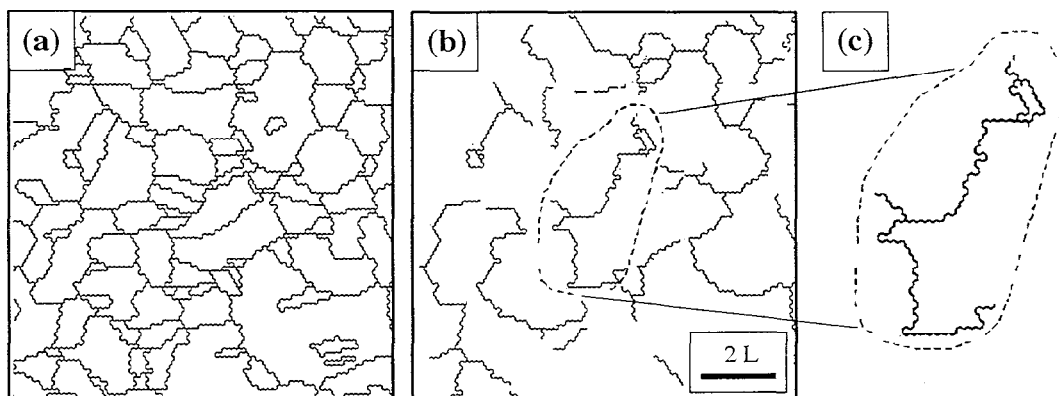


Fig. 2: Example of the cluster identification process, showing (a) the full network of grain boundaries, (b) only the random high-angle boundaries, and (c) an example of a single interconnected random boundary cluster.

of N discrete components (i.e., boundaries or boundary segments), the radius of gyration R_g of a cluster is defined in terms of the average distance of a boundary from its center of mass, \mathbf{r}_o , as follows:

$$R_g^2 = \frac{1}{N} \sum_{i=1}^N |\mathbf{r}_i - \mathbf{r}_o|^2 \quad (1) \quad \text{and} \quad \mathbf{r}_o = \frac{1}{N} \sum_{i=1}^N \mathbf{r}_i \quad (2)$$

where \mathbf{r}_i is a vector pointing to the position of the i^{th} boundary or boundary segment. An additional length scale of interest is the maximum linear dimension of a cluster, D , which may govern the length of intergranular cracks (note again that D is normalized by the mean linear intercept length).

The above properties describe individual clusters; average measures of the entire cluster population may be more representative of the microstructure. The weighted average cluster mass and the *correlation length*, which is effectively a weighted average diameter of gyration, are given by (3) and (4), respectively:

$$\langle s \rangle = \frac{\sum_s s^2 \cdot n_s}{\sum_s s \cdot n_s} \quad (3) \quad \text{and} \quad \xi^2 = \frac{2 \cdot \sum_s R_g^2 \cdot s^2 \cdot n_s}{\sum_s s \cdot n_s} \quad (4)$$

where n_s is the cluster mass distribution function, which gives the number of clusters of size s per unit area [10].

As described above, the maximum linear dimension of clusters is important as regards the extent of, e.g., intergranular crack propagation. This and other percolation-sensitive material properties are sensitive to the dimension of the largest cluster; we accordingly also identify the largest linear dimension of any cluster in a given specimen, D_{max} .

The cluster mass distribution described above, n_s , gives the number density of clusters of mass s . In a given specimen, the mass fraction of clusters of mass s is given as:

$$m_s = \frac{s \cdot n_s}{\sum_s s \cdot n_s} \quad (5)$$

For a quantitative comparison among different specimens with different processing histories, it is important that the data sets are of comparable size and shape. Therefore, for all of the specimens investigated here, the analyzed EBSD data sets were chosen such that they were: (i) nearly square, with aspect ratios between 1.0 and 1.1, and (ii) all of the same size in dimensionless units, spanning about 632 grains on each specimen.

Fig. 3 shows the evolution of the grain boundary network as a function of processing cycle, extracted from much larger EBSD data sets; Figs. 3a-c show only the random boundaries, while Figs. 3d-f show the complementary special boundaries. In this figure, the individual pictures are all scaled to the mean linear intercept length. Qualitatively, Fig. 3 shows the fragmentation of the random boundary network as the special fraction is increased through grain boundary engineering. Additionally, Figs. 3d-f show the gradual development of interconnected networks of special boundaries as a consequence of such processing. After four processing cycles (Figs. 3c and 3f), the random boundary network is locally interrupted by special boundaries in many locations.

The changes in the grain boundary network structure described above and shown in Fig. 3 can be quantified using cluster analysis. Fig. 4 shows the mass fraction, m_s , for clusters of size s in Inconel 600, as a function of processing history. In percolative systems, cluster masses tend to be distributed across several orders of magnitude, particularly near the percolation threshold [10]. Therefore, the data in Fig. 4 have been collected in bins spaced evenly in $\log(s)$; the size s on the x-axis in this figure represents the upper bound of each bin. Physically, Fig. 4 indicates

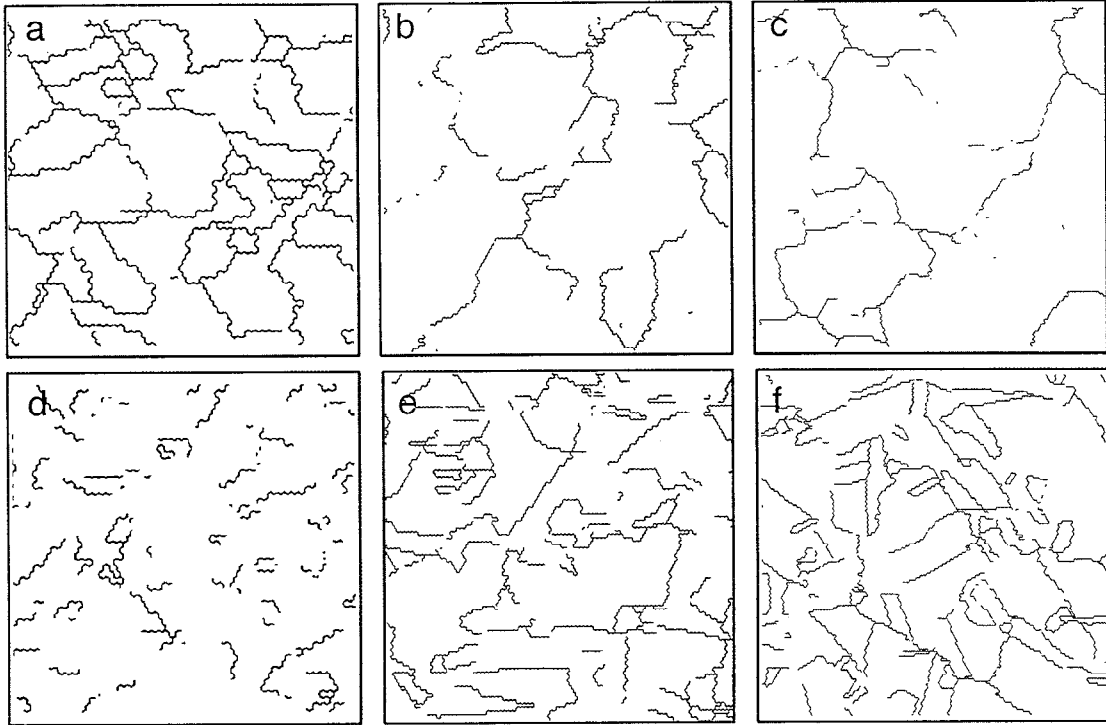


Fig. 3: Qualitative illustration of the changing network topology during grain boundary engineering; (a)-(c) show only the random boundaries after 0, 2, and 4 cycles, respectively, and (d)-(f) show only the special boundaries from the same area, again as a function of the number of processing cycles.

what fraction of the total length of boundaries in the specimen is occupied in clusters of size s . For example, Fig. 4a pertains to the random boundary clusters in the as-received material, where the majority of boundaries are incorporated into a single large cluster of mass 391 units, i.e., spanning hundreds of grains. As also observed qualitatively in Fig. 3a, the large random boundary clusters in the as-received specimen are highly interconnected and percolate through the 2-D area of observation. The distribution functions presented in Fig. 4 thus give a quantitative interpretation of the qualitative trends observed in Fig. 3. Before proceeding, it is important to note that there are errors of truncation for clusters that cross the edges of the data set. This type of error particularly affects the mass of very large clusters and the reported masses of the largest clusters, which are only observed in random boundaries of the as-received material, should be regarded as a lower bound on the true cluster mass.

In Figs. 4a-c, the effect of grain boundary engineering on random boundary clusters is shown quantitatively. After just two cycles of processing (Fig. 4b), the largest interconnected clusters of random boundaries are broken up, and the largest clusters have mass less than 100 units. On each subsequent processing cycle, the random boundary network becomes increasingly fragmented, and larger populations of small clusters emerge. After four processing cycles (Fig. 4c), all of the clusters have mass below 32 units, more than an order of magnitude smaller than the largest cluster mass in the as-received condition. Although there has been considerable discussion surrounding the connectivity of random grain boundaries during grain boundary engineering, these results are, to our knowledge, the first direct quantitative measurement of such connectivity and its evolution as a function of processing history. The

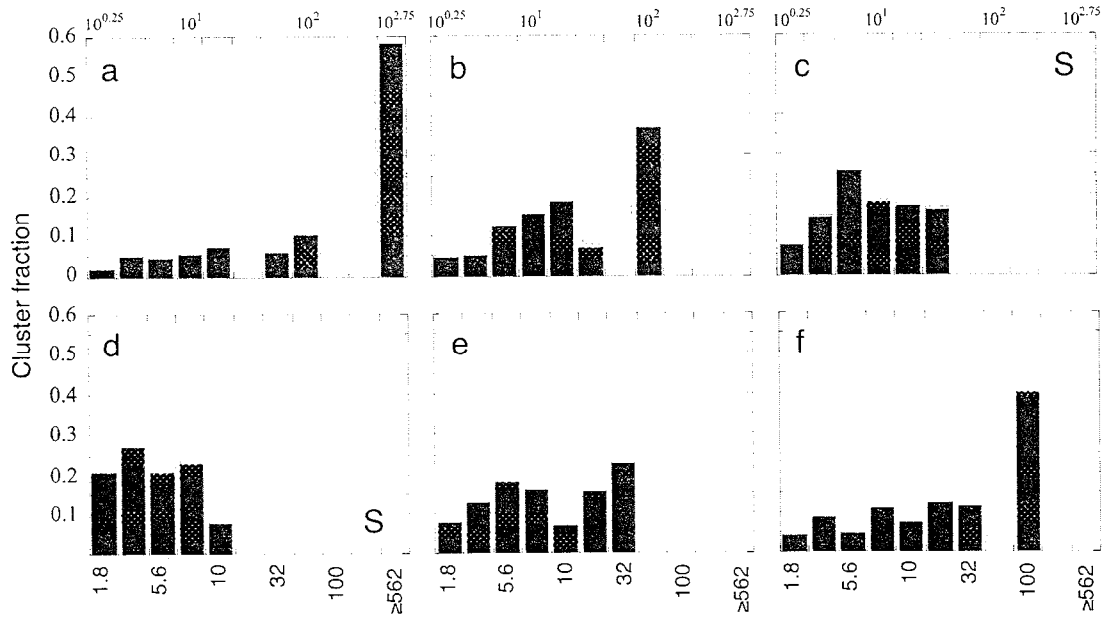


Fig. 4: Quantitative depiction of the changing network topology during grain boundary engineering; (a)-(c) show the cluster mass distributions for only the random boundaries after 0, 2, and 4 cycles, respectively, and (d)-(f) show the complementary mass distributions for the special boundary clusters.

dramatic fragmentation of the random boundary network documented in Fig. 4 lends support to the speculations of previous authors and may explain the concomitant remarkable improvements observed in material properties after grain boundary engineering.

Figs. 4d-f show the mass distributions for clusters of special grain boundaries, and therefore represent the complement to Figs. 4a-c for the random boundary clusters. In the as-received state, special clusters are extremely small and isolated (Fig. 4d), as also observed qualitatively in Fig. 3d. With each cycle of processing, the connectivity of the special boundaries improves, and after four processing cycles, the largest fraction of boundaries is of mass 100-178 units. Compared with the as-received material, this is an order of magnitude increase in the maximum cluster mass. Thus, the order-of-magnitude decrease in random cluster mass is symmetrically offset by a 10-fold increase in the mass of special clusters.

The cluster mass changes illustrated in Fig. 4 are accompanied by changes in the length scales of the clusters. The decrease

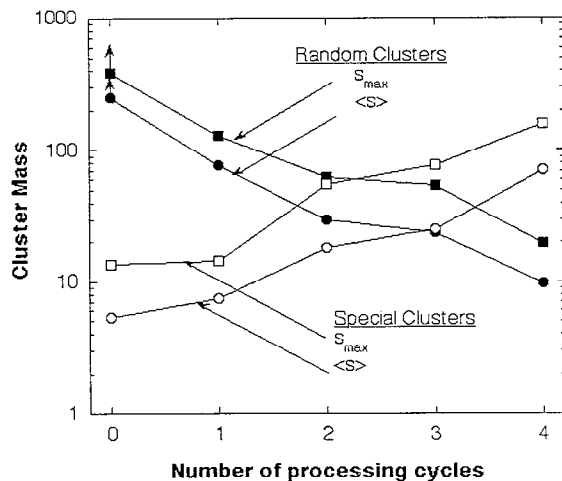


Fig. 5: Changes in the characteristic length scales of clusters, including the maximum cluster dimension (D_{max}) and the correlation length (ξ , Eq. (4)) for random and special boundary clusters.

in random cluster size and the corresponding increase in special cluster size during sequential thermomechanical processing are shown in Fig 5. The maximum linear cluster dimension, D_{\max} , represents a projection of the largest contiguous path of random or special boundaries in the two-dimensional section, while the correlation length ξ is a representation of the average diameter of all clusters measured in a given specimen. Again, we note that these length scales are dimensionless, being normalized by the 2-D grain size. As expected from the trends observed in cluster mass, the process of grain boundary engineering leads to a significant reduction in the random boundary cluster size, by about a factor of three.

The Non-Random Nature of Grain Boundary Networks

The microstructural inversion described above, from random to special grain boundary networks, appears to be generally symmetric when the quantitative data in Figs. 4 and 5 are examined. However, visual inspection of the network topology in Fig. 3 indicates that there are significant topological differences between the special and random boundary clusters. These differences are particularly apparent when comparing Figs. 3c and 3d, which show, respectively, the random boundaries after processing and the special boundaries in the as-received material. The cluster mass distributions in these two conditions are quantitatively similar, as shown in the corresponding frames of Figs. 4c and 4d. However, these two states are topologically very different. The special boundaries in Fig. 3d appear well dispersed, as though they had been placed into the microstructure by a random process. In contrast, the random boundary clusters in Fig. 3c appear to be aligned with one another, and to outline a larger structure of grains. In fact, the topology of the random boundaries in Fig. 3c suggests that a large network of random grain boundaries has been broken into small clusters only by removing short segments from the network. This unique topology is probably due to the formation of twins during grain boundary engineering [3,7,11] in which annealing twins often form as parallel coherent $\Sigma 3$ boundaries within a grain. At the grain edge where the twin boundaries terminate, the grain boundary character is changed according to the Σ -product rule [12]. In many cases, this results in a short segment of special boundary that divides a random boundary into two unconnected segments. Multiple twinning induced by sequential processing can interrupt the random network in many isolated places, and thereby reduce the random cluster size. However, these small interruptions produce a highly non-random topology of the random boundaries, as observed in Fig. 3c.

Figs. 3b and 3e provide a further example of topological differences between random and special boundary clusters. These figures correspond to a special number fraction near $f_n = 0.5$, so approximately half of the boundaries are special and half are random. In this condition, a random percolation process would lead to essentially identical topologies for the two cluster populations. However, the random and special clusters are qualitatively very different (Figs. 3b and 3e). These observations strongly suggest that the microstructure cannot be regarded as a random percolation problem based solely upon the special boundary fraction, and emphasize the topological uniqueness of grain boundary engineered microstructures, which entail constraints at grain triple junctions. As new analysis strategies for EBSD become standardized, these data sets can reveal subtle details of connectivity among grain boundary networks, and microstructural rankings can be founded upon topological information.

Acknowledgments

The authors wish to acknowledge Lan Nguyen at Lawrence Livermore National Laboratory for the processing and metallography of samples used in this study. This work was performed under the auspices of the U.S. DOE by the University of California, Lawrence Livermore National Laboratory under contract W-7405-Eng-48.

References

1. Wells, D. B., Stewart, J., Herbert, A. W., Scott, P. M., and Williams, D. E., 1989, *Corrosion*, 45:649.
2. Palumbo, G., King, P. J., Aust, K. T., Erb, U. and Lichtenberger, P. C., 1991, *Scripta Metall. Mater.*, 25:1775.
3. Gertsman, V. Y. and Tangri, K., 1995, *Acta Metall. Mater.*, 43:2317.
4. Wright, S. I., 2000, in Electron Backscatter Diffraction in Materials Science (eds. A. J. Schwartz, M. Kumar and B. L. Adams), New York:Kluwer Academic/Plenum Publishers, p. 51.
5. Kumar, M., King, W. E. and Schwartz, A. J., 2000, *Acta Mater.*, 48:2081.
6. Schuh, C. A., Kumar, M. and King, W. E., 2002, *Acta Mater.*, in press.
7. Kumar, M., Schwartz, A. J. and King, W. E., 2002, *Acta Mater.*, 50:2599.
8. Gertsman, V. Y., Janecek, M. and Tangri, K., 1996, *Acta Mater.*, 44:2869.
9. Sedgewick, R., 1988, *Algorithms* (Reading, MA: Addison-Wesley).
10. Stauffer, D. and Aharony, A., 1992, *Introduction to Percolation Theory* (London: Taylor and Francis).
11. Lin, P., Palumbo, G., Erb, U. and Aust, K. T., 1995, *Scripta Metall. Mater.*, 33:1387.
12. Miyazawa, K., Iwasaki, Y., Ito, K. and Ishida, Y., 1996, *Acta Crystallographica*, A52:787.